

Development of a Colorimetric Polydiacetylene Nanocomposite Fiber Sensor for Selective Detection of Organophosphate Pesticides

A K M Mashud Alam and Chunhui Xiang*



Cite This: *ACS Omega* 2025, 10, 12346–12356



Read Online

ACCESS |



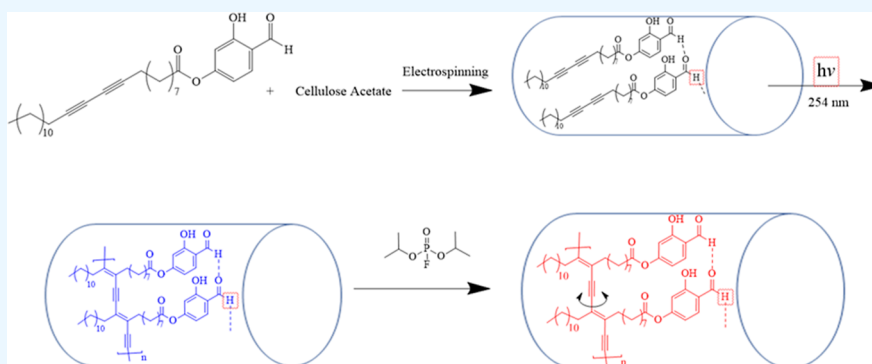
Metrics & More



Article Recommendations



Supporting Information



ABSTRACT: Exposure to organophosphate (OP) pesticides is highly hazardous to human health and well-being. It has been linked to over 250,000 annual deaths connected to various chronic diseases, including cancer, Parkinson's, Alzheimer's, depression, etc. In the absence of any solid-state sensing system suitable for integration into a clothing system, an equipment-free on-site detection system for OP insecticides is essential for mitigating the severe health risks from OP exposure. This work demonstrates the synthesis, fabrication, and naked-eye and quantitative detection of OP insecticides with a polydiacetylene (PDA) ester containing the nanocomposite fiber sensor. Ester of PDA (PDA–HBA) was synthesized via facile green chemical synthesis and incorporated into a cellulosic nanocomposite fibrous assembly via the electrospinning technique. The solid-state soft sensor exhibited a blue-to-pink/red color transition within seconds of exposure to OP pesticide diisopropylfluorophosphate (DFP), and the color change was visible to the naked eye. Nanocomposite fibers containing 10% PCDA–HBA were found to be the optimum composition for DFP detection. The limit of DFP detection was 63 ppm. Scanning electron microscopy, energy-dispersive X-ray spectroscopy, wide-angle X-ray diffraction (XRD), small-angle XRD, nuclear magnetic resonance, and Fourier-transform infrared spectroscopy were employed for characterization. This research is a landmark study in the development of a highly sensitive and selective OP sensing system.

Pesticides have been widely used throughout the world to protect crops from insects and increase agricultural output.¹ Organophosphates (OP) are the most widely used insecticides today. They are used in agriculture, homes, gardens, and veterinary practices. Exposures to pesticides occur in the agricultural workplace during production, transportation, preparation (mixing and loading), and application (spraying).^{2,3} Diseases including cancer, leukemia, diabetes, Parkinson's, depression, autism, asthma, and differential DNA methylation have been linked to pesticide exposure.^{4,5} Most affected individuals were exposed to insecticides, with OPs being the most impactful class of pesticides.⁶ Therefore, pesticide detection, especially of OPs, can play an important role in mitigating the negative consequences of pesticide contamination.

Conventional chromatographic techniques, including high-performance liquid chromatography (HPLC), gas chromatography, and mass spectrometry (MS), have traditionally been used for pesticide detections. Although these techniques offer

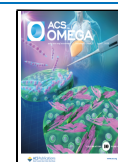
robust trace analysis with excellent sensitivity and high reproducibility, many drawbacks include sophisticated equipment, experienced operators, and tedious and time-consuming sample preparation. Moreover, they are not available in many parts of the world and are not suitable for on-site and real-time applications. Therefore, developing alternative strategies for simple, quick, sensitive, selective, accurate, less expensive, and user-friendly techniques would be highly beneficial in detecting harmful pesticides.^{7–9} Among the alternatives, optical sensors are a facile, rapid, and low-cost approach for the sensitive detection of OP pesticides. Generally, an optical sensor

Received: December 17, 2024

Revised: January 23, 2025

Accepted: February 20, 2025

Published: March 19, 2025



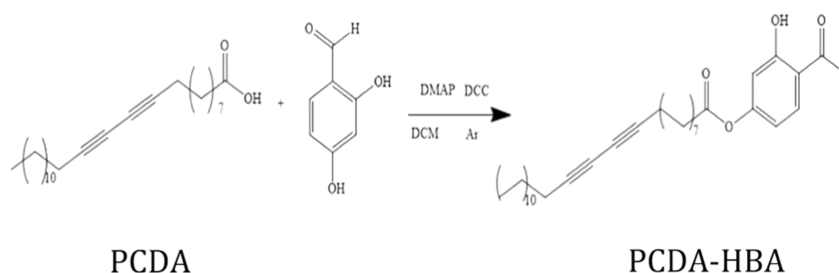


Figure 1. Synthetic scheme for the functionalization of PCDA into PCDA–HBA.

contains a recognition unit to interact with the target pesticide and a transducer component for signaling the binding event.⁷ The current well-established optical probes are categorized into four broad categories based on signal output formats, such as colorimetric (CL), fluorescence (FL), surface-enhanced Raman spectroscopy, and chemiluminescence sensor. The output signal could be CL, fluorometric, or a combination.

CL detection has been attractive due to its ease of use, quick response, equipment-free detection, and cost-effectiveness. The color change caused by a chemical interaction can be visualized by the unaided eye, therefore omitting the necessity to use any instrument.⁷ This detection technique has been a preferred method for a “yes/no” answer or semiquantitative result. The direct visualization of the response signal (output) eliminates the requirement of any additional transduction element, making them highly interesting for developing smart devices for point-of-care applications.¹⁰ Therefore, the key challenge for fabricating a CL sensing platform is transforming the response behavior into a visual color change. Several techniques have been employed for developing a CL sensing platform, including functional polymers, metal nanoparticles, artificial enzymes called nanozymes, etc.

Recently, a very interesting functional polymer called polydiacetylene (PDA), a π -conjugated polymer extensively studied for various sensing applications, has been explored for OP pesticide sensing.¹¹ PDAs are usually prepared via 1,4 addition photopolymerization of self-assembled diacetylene (DA) monomers such as 10,12-pentacosadiynoic acid (PCDA). Due to the amphiphilic nature, DAs in liquid medium form intermolecular packing via hydrophobic–hydrophobic interactions of adjacent tails. The self-assembled monomers are photopolymerized by UV light or γ -ray irradiation without using any chemical initiators or catalysts, resulting in a highly ordered conjugated backbone. After photopolymerization, PDAs exhibit a blue color with a maximum absorption (λ_{max}) at 640 nm. They are especially attractive because they exhibit a blue-to-red color transition, visible to the naked eye when subjected to external stimuli.¹² The red phase shows an absorption peak (λ_{max}) at around 540 nm. Many research groups around the globe have been investigating the color-transition properties of PDAs. However, the researchers are not yet in a common opinion of the sensing mechanism.¹³ The external stimuli disrupt the polymer chain conformation of PDA, altering the electronic states of the conjugated backbone. These changes broaden the energy gap, leading to a corresponding color transformation.¹⁴

To achieve better sensitivity and selectivity, PDAs have been functionalized with a wide range of functional groups for the detection of an array of analytes, such as metal ions,¹⁵ surfactants,¹³ enzymes,¹⁶ amino acids,¹⁷ gas molecules,¹⁸ viruses,¹⁹ bacteria,¹⁹ etc. Inspired by the antidotes of OP,

functionalized PDAs have recently been explored to detect OPs in liquid medium.^{12,20} However, a solid-state sensing system for OP pesticide diisopropylfluorophosphate (DFP) in bulk, micro-, or nanostructure is scarce in the literature. Therefore, this research is focused on developing a solid-state nanocomposite fiber (NCF)-membrane-based DFP sensing system. The sensing platform could be promising due to the nanoscale size, lightweight, porous structure, high surface area-to-volume ratio, and high target specificity in monitoring DFP with greater precision and lower detection limits.²¹

In this study, an NCF-membrane-based PDA ester-incorporated pesticide sensor for the detection of OP pesticide DFP was developed. PDA ester was synthesized following green chemistry. Cellulose acetate (CA) was chosen as the matrix polymer for fiber development since it can be easily hydrolyzed to regenerated cellulose (RC), having a large number of exposed hydroxyl (OH–) groups on the fiber structure that enhance the sensitivity of detection. The electrospinning technique was employed for fabricating NCF membranes since it fabricates fibers with high specific surface area and high porosity that facilitate superior sensitivity to thin film structures.²² OP pesticide DFP was employed as a model pesticide stimulus.²³ The sensitivity, selectivity, and limit of detection (LOD) of the nanocomposite sensors were studied by using membranes having various PDA ester loading. Characterization techniques such as scanning electron microscopy (SEM), energy-dispersive X-ray spectroscopy (EDS), wide-angle X-ray diffraction (XRD), small-angle XRD (SAXS), nuclear magnetic resonance (NMR), Fourier-transform infrared spectroscopy (FT-IR), and UV–vis spectroscopy were used to study the sensing mechanism further.

MATERIALS AND METHODS

Materials. PCDA (98%) was purchased from GFS Organics (Columbus, OH, USA). CA with 39% acetyl content and \overline{M}_n of 30 kDa, determined by gel permeation chromatography, was purchased from Sigma-Aldrich (St. Louis, MO, USA). 2,4-Dihydroxybenzaldehyde (98%), 4-(dimethylamino) pyridine (DMAP, $\geq 99\%$), *N,N'*-dicyclohexylcarbodiimide (DCC, 99%), and sodium hydroxide ($\geq 97\%$) were also purchased from Sigma-Aldrich. Certified ACS grade acetone ($\geq 99.9\%$), acetonitrile ($\geq 99.9\%$), ethyl acetate (99.5%), hexane (95%), hydrochloric acid (HCl) (38.8%), deionized (DI) water (HPLC grade), and methylene chloride (99.8%) were purchased from Fisher Chemical (Fair Lawn, NJ, USA).

Methods. *Synthesis of Aldehyde-Functionalized PCDA Ester (PCDA–HBA).* The synthesis of PCDA–HBA was carried out based on our previously reported method.²⁴ The synthetic scheme is depicted in Figure 1. In summary, PCDA (4 mmol), 2,4-dihydroxybenzaldehyde (4 mmol), and DMAP (1 mmol)

were combined in a light-protected round-bottom flask. The mixture was dissolved in 100 mL of dichloromethane and sparged with argon. A 15 mL solution containing 2 mmol of DCC was slowly added to the solution by syringe and continued stirring on a hot plate stirrer for 24 h at room temperature. Dicyclohexylurea, the reaction byproduct, was filtered off by gravity filtration. The solvent was removed under a vacuum on a rotary evaporator (BUCHI Rotavapor, Model R-200, BUCHI Co., New Castle, DE, USA) and yielded a tan solid. The residue was purified by column chromatography with 10:1 hexane: ethyl acetate, and the desired DA monomer PCDA–HBA was obtained as a white solid. At room temperature, the structure was confirmed with NMR (HNMR) (Varian MR 400, Varian, Palo Alto, CA). The materials, protected from light and air, were stored in a freezer.

Fabrication of the NCFs. Preparation of the electrospinning solution. The electrospinning solution was prepared in two steps by incorporating the sensing polymer PCDA–HBA and matrix polymer CA in acetone. First, a 15% (w/v) solution of CA was prepared by dissolving CA in acetone. Then, the required amount of PCDA–HBA (5, 10, 15, and 20 w/w %) based on the weight of CA was added to the CA solution (Table 1). The resulting mixture was kept under constant

Table 1. Electrospinning Design of CA–PCDA–HBA Composite Fibers

CA (w/v) %	PCDA–HBA (% CA)	voltage (kV)	distance (cm)	injection speed (mL h ^{−1})	fiber ID
15	5	15	10	1	HBA-5
15	10	15	10	1	HBA-10
15	15	15	10	1	HBA-15
15	20	15	10	1	HBA-20

stirring overnight in a light-protected container with a Burrell wrist-action shaker, model 75 (Burrell Scientific LLC, Pittsburgh, PA, USA), at room temperature to obtain a homogeneous CA–PCDA–HBA solution ready for electrospinning.

Electrospinning. A freshly prepared CA–PCDA–HBA solution was loaded into a 10 mL plastic syringe attached to a stainless-steel needle having an inner diameter of 0.8 mm. The solution was then continuously fed at a fixed rate of 1 mL h^{−1} by a syringe pump (Harvard Apparatus, Holliston, MA, USA). A DC power supply instrument applied a fixed electric potential of 15 kV between the needle tip and the collector (Gamma High Voltage Research, FL, USA). The collector was placed 10 cm apart from the needle tip. The electrospinning process was continued for two (2) h under ambient conditions to obtain a thick colorless fiber membrane.

Deacetylation of CA–HBA into RC–HBA. The deacetylation was conducted to remove acetyl groups from CA–PCDA NCF membranes following previously reported methods.²⁵ Deacetylation solution comprising 4:1 NaOH/EtOH was made using 0.1 M NaOH in DI water. CA–PCDA NCF membranes sandwiched between glass fiber mesh were soaked in a glass bowl in a deacetylation solution. A magnetic stirring bar placed on the mesh was kept rotating at 150 rpm for 30 h at room temperature on a hot plate. The membranes were then thoroughly rinsed with DI water to complete neutralization, as confirmed by pH paper. They were then air-dried overnight, followed by vacuum drying at 60 °C for 24 h to obtain regenerated cellulosic RC–PCDA NCF membranes. The RC–

PCDA NCF membranes were then stored in a dark place away from light. The change in the chemical structure of the nanocomposites was evaluated with FT-IR.

Photopolymerization of the RC–HBA NCF Membranes. The RC–HBA NCF membranes were photopolymerized with 254 nm UV-light (Spectroline, Longlife filter, New York, USA) irradiation for 1 min on both sides of the membranes. During UV irradiation, the colorless fibers turned blue within 30 s, turning into deep blue RC–PDA composites in 1 min.

Characterization of NCF Membranes. NMR spectroscopy, a Varian MR-400 M spectrometer, and a narrow bore 9.4 T/400 MHz magnet equipped with a one NMR pulse-field gradient probe were used to analyze the chemical composition of the PCDA–HBA crystals. Solid-state nanocomposite membranes (blue and red) were soaked in methyl alcohol D4 solvent in Oakton sample bottles to leach out the PCDA–HBA from the HBA-10 nanocomposite membranes. The samples were then sonicated for 5 min. The solvent was then transferred to NMR tubes for characterization. Chemical shifts were reported in ppm from the solvent resonance following the internal standard. Multiplicity is indicated as follows: s (singlet), d (doublet), t (triplet), and m (multiplet).

Scanning Electron Microscopy. A field emission scanning electron microscope (FEI Quanta 250 FE-SEM) was employed to study the size and surface morphology of the nanocomposite membranes. The membranes were kept under a vacuum overnight to evaporate any residual solvent or moisture. They were then sputter-coated with a 5 nm layer of iridium to improve the conductivity of the samples for improved imaging. Image J software (National Institute of Health, USA) was used to calculate the diameter and distribution of the fibers. The average and distribution of the diameters were determined by measuring 50 representative fibers from the SEM images.

Energy-Dispersive X-Ray Spectroscopy. EDS analyses were conducted with a JEOL JSM-IT200 (Peabody, MA, USA) SEM–EDS on the untreated (control) and DFP-treated nanocomposite membranes to compare the morphology and elemental and chemical analyses of the sample surfaces before and after the CL transition. The SEM images were taken at an acceleration voltage of 20 kV and a magnification level of 5.0 K.

Wide-angle XRD. Wide-angle XRD measurements were recorded on a Rigaku Ultima IV X-ray diffractometer (XRD) (Tokyo, Japan) in the range $2\theta = 10$ – 60° with a step size (2θ) of 0.02. Data were collected with Cu K α —radiation $\lambda = 1.54178$ nm with a graphite monochromator. The blue and red phases of the nanocomposite membranes were compared using XRD analysis.

Small-Angle XRD. Small-angle X-ray scattering (SAXS) analysis of the NCF membranes was carried out with a Xenocs Xeuss 2.0 small angle X-ray scattering instrument (Grenoble, France) with a Cu K α source ($\lambda = 1.54$ Å). The sample chamber was kept under a vacuum at room temperature. Detection of X-rays was made with a Pilatus 1 M detector. The sample-to-detector distance was calibrated with silver behenate powder to be 1980 mm. The scattering pattern from the red sample was acquired with the line-eraser mode.

FT-IR Spectroscopy. An Agilent Cary 630 FT-IR spectrometer was purchased from Agilent Technologies, Inc. (Danbury, CT, USA), equipped with a DATR accessory was used to study the development of RC from CA. Before FT-IR analysis, all NCF membranes were dried overnight at room

temperature in an Isotemp (model 282A) programmable vacuum oven (Fisher Scientific, MA). In order to run the experiments, air was used as a background before taking the IR of the samples. Samples were scanned 32 times at 4 cm^{-1} resolution with an interval of 1 cm^{-1} over wavenumbers of $750\text{--}4000\text{ cm}^{-1}$.

UV–Visible Spectroscopy. The CL properties of the composites were measured with a UV–vis spectrophotometer (Nicolet Evolution 300 UV–vis, Thermo Scientific, Waltham, MA, USA) at room temperature. The solvent was removed from the composites by drying them overnight at $40\text{ }^{\circ}\text{C}$ in a vacuum oven (Fisher Scientific, Maltham, MA, USA). The absorption spectra of the nanofiber (NF) composites were collected in the range of $400\text{--}800\text{ cm}^{-1}$ wavelength before and after the treatment with DFP. From the intensity value of the spectra before and after the color change, the CL response (% CR) value was calculated using eq 1 as below

$$\% \text{ CR} = \left[\frac{\text{PB}_{\text{before}} - \text{PB}_{\text{after}}}{\text{PB}_{\text{before}}} \right] \times 100 \quad (1)$$

where the $\text{PB}_{\text{before}}$ and PB_{after} are the respective percent blue (PB) of the composites before and after the color change, respectively. The PB values were calculated by following eq 2

$$\text{PB} = \left[\frac{A_{\text{blue}}}{A_{\text{blue}} + A_{\text{red}}} \right] \times 100 \quad (2)$$

where A_{blue} and A_{red} are the absorbances at 640 and 560 nm, respectively.

Test of Sensitivity to OP Pesticide, DFP. RC–PDA NCF membranes encapsulated with a varied amount of functionalized PDA esters (PDA–HBAs) were exposed to DFP solution in acetone at concentrations ranging from 10 to 600 mmol in a fume hood. 2 mL of diluted DFP solution were poured onto each type of nanocomposite and observed for 2 h for color transition.

Test of Selectivity. The selectivity of the developed detection system was examined by using some carefully selected potential interferents such as acetone, acetonitrile, water, and HCl to eliminate any possible false alarms of the detection.^{12,20} This test was planned to examine whether any solvent or byproduct induced the color change or if it was highly selective to DFP only. Acetone, acetonitrile, and DI water were used as purchased, and HCl was diluted to 0.6 M in DI water. 2.0 mL of the above chemicals were poured onto the HBA-10 NCF membranes and observed for color transition for an hour. Photographs were captured after the samples were air-dried.

RESULTS AND DISCUSSION

Synthesis of Aldehyde-Functionalized PCDA Ester (PCDA–HBA). Dihydroxy benzaldehyde was conjugated with an pentacosadiynoic acid terminus, as depicted in Figure 1, to functionalize the PCDA macromolecule into PCDA ester (PCDA–HBA), following our previously reported synthetic method.²⁴ The ^1H NMR spectra of PCDA, 2,4-dihydroxybenzaldehyde, and PCDA–HBA, as recorded on a 400 MHz instrument using $\text{DMSO-}d_6$ as the solvent, are presented in Figures S1–S3. The peaks are assigned as follows: ^1H NMR (400 MHz, $\text{DMSO-}d_6$): δ 0.85 (t, 3H), 1.23–1.63 (m, 32H), 2.26 (t, 4H), 2.51 (t, 2H), 6.68–6.75 (m, 2H), 7.68 (s, 1H), 10.21 (s, 1H). The peak at 0.85 ppm represents the methyl

($-\text{CH}_3$) group; multiple peaks between 1.23 and 1.63 ppm represent the methylene group ($-\text{CH}_2-$) of the hydrocarbon chain; peaks at 2.26 and 2.51 ppm represent the methylene group adjacent to the alkyne ($-\text{C}\equiv$) group; peaks between 6 and 8 ppm in spectrum B belong to the protons attached to the aromatic ring, and the peak at 10.21 ppm represents the aldehyde group. Comparing and calculating the spectra A, B, and C, the spectrum C confirms the presence of the aldehyde functionalized PCDA ester, PCDA–HBA.²⁴ The spectra of PCDA and PCDA–HBA are consistent with the previously published literature.²⁰

Fabrication of NCF Membranes Containing PCDA Ester. The fabrication of NCF using the electrospinning technique is critical and requires precise control over the chemical composition and processing parameters. Factors including the polymer molecular weight, solution concentration, solution viscosity, conductivity, solvent surface tension, vapor pressure, solubility have been influential in the fabrication and morphology of NCF.¹¹ Electrospinning of PCDA ester alone is highly challenging due to its low viscosity in solution. Therefore, a high-viscosity supporting polymer matrix was used to facilitate electrospinning. CA was chosen as a matrix polymer for electrospinning due to its excellent mechanical and chemical properties, biodegradability, non-toxicity, and low cost.^{26–28} Acetone, a low surface tension (22.7 mN/m) solvent, was used due to its compatible solubility parameters (9.8 J/cm^3) with CA.²⁹

Among the critical electrospinning parameters, injection rate, tip-to-collector distance, and applied voltage were kept constant based on the results of several preliminary experiments designed with varied injection rates ranging from 1 to 3 mL h^{-1} , tip-to-collector distance ranging from 5 to 20 cm, and applied voltage ranging from 10 to 25 kV at concentrations ranging from 12 to 17% (w/v). Based on these experiments, this study found a combination of a 1 mL h^{-1} injection rate, a 10 cm tip-to-collector distance, and a 15 kV applied voltage optimal for electrospinning. A 15% CA concentration, optimal for forming defect-free continuous fibers, was kept fixed, and the required amount of PCDA–HBA was added to the weight of CA. The effects of the amount loading of PCDA–HBA were studied in this research. The addition of an increased amount of PCDA–HBA in the CA solution (Table 1) resulted in a reduction in the viscosity of the solution compared to the pure CA solution. The variation in viscosity, along with other processing parameters, resulted in the formation of fibers with varying diameters and morphologies.

Figure 2 exhibits the SEM images of the NCFs as spun (CA–HBA) and after deacetylation/hydrolysis (RC–HBA). The CA–HBA fiber composites, irrespective of the PDA–HBA loading, are defect-free and fluffy, showing less interfiber adhesion due to the presence of a charged acetate group on the fiber surface.³⁰ The average diameter of the fiber composites (CA–HBA) was calculated as 1.67 ± 1.1 , 0.82 ± 0.47 , 0.92 ± 0.44 , and $0.95 \pm 0.70\text{ }\mu\text{m}$, respectively, for HBA-5, HBA-10, HBA-15, and HBA-20. However, other researchers reported that fibers became flatter after deacetylation/hydrolysis (RC–HBA). Interfiber adhesion increased significantly due to the increase in hydroxyl groups on the fiber surface owing to the chemical treatment.

Regeneration of CA–HBA Nanocomposite Membranes into RC–HBA Membranes. The regeneration of cellulose nanocomposites (RC–HBA) from the as-spun CA nanocomposites (CA–HBA) was done via a hydrolysis

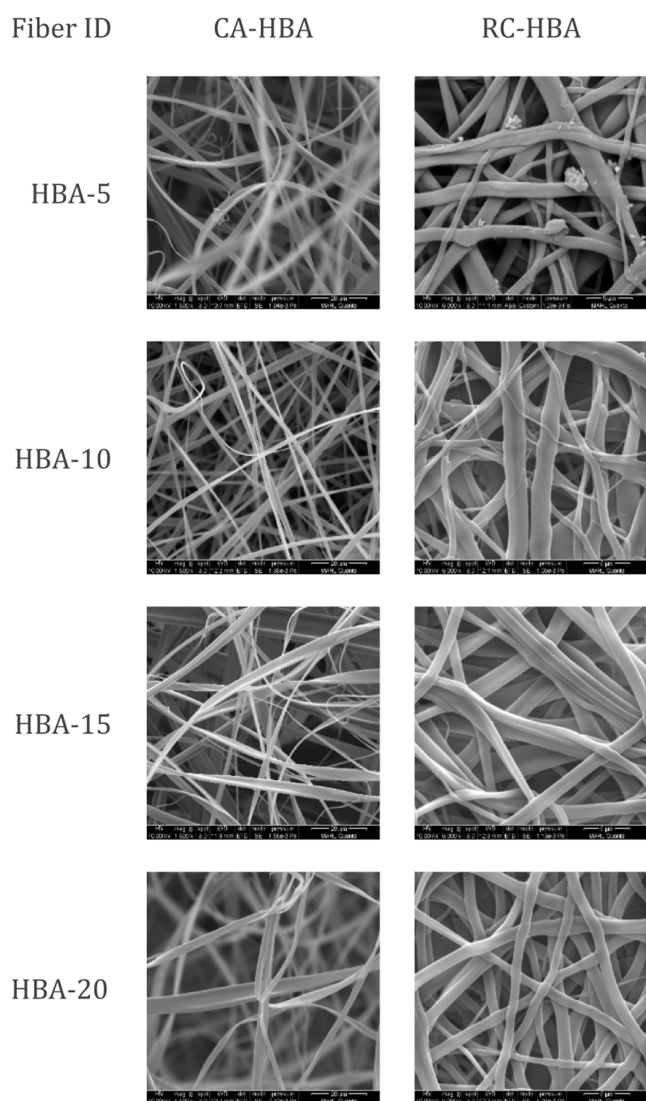


Figure 2. SEM images of the fiber composites before (CA-HBA) and after (RC-HBA) hydrolysis treatment.

treatment. FT-IR was conducted to compare the PCDA-HBA crystal with RC-HBA NCF membranes to determine whether the matrix polymer and the hydrolysis treatment affected the conjugated macromolecules that might hinder the sensing properties of the RC-HBA NCFs.

Spectrum A of Figure 3 represents the PCDA-HBA crystal, where the following resonance features were interpreted for

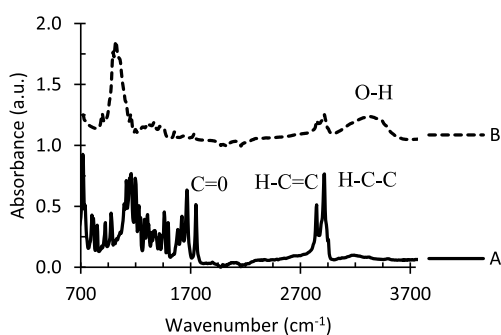


Figure 3. FT-IR spectra of the PCDA-HBA crystal (A) and RC NCF HBA-10 (B).

characterization: IR ν_{\max} (cm^{-1}): 2914 (aldehydic H-C=O stretch), 2843 (aldehydic H-C-H stretch), 1747 (ester, C=O stretch), 1460 (aldehydic C-H stretch bending), and 1155 (C-O stretch). The spectrum agrees with the predicted structure of PCDA-HBA, and the resonance features are similar to those previously reported for PCDA-HBA.³¹ The two peaks for C-H bonds between 2800 and 2950 and the carbonyl (C=O) peak around 1750 suggest that an aldehyde group has been added to the PCDA structure. The characteristic vibration band adjacent to the carbonyl bond around 1600 cm^{-1} shows the stretching motion of a benzene ring in the structure. The vibration of the C(sp²)-H bond near 3000 cm^{-1} also indicates the presence of a benzene ring in the structure.

Spectrum B represents the PCDA-HBA-encapsulated RC NCFs RC-HBA. The resonance features observed were as follows: ν_{\max} (cm^{-1}): 3350 (O-H), 2921 (aldehydic H-C=O stretch), 2854 (aldehydic H-C-H stretch), 1740 (ester, C=O stretch), 1430 (aldehydic C-H stretch bending), and 1020 (C-O stretch). Similar IR spectra between the PCDA-HBA crystal and RC-HBA demonstrate that PCDA-HBA retains its functional groups in the matrix polymer structures despite the deacetylation process. In the RC-HBA structure, the carbonyl (C=O) peak shifted toward a lower wavenumber, which indicates that the CO group has decreased as a result of hydrolysis. Following hydrolysis, the broad absorption peak at 3350 cm^{-1} indicates a large amount of hydroxyl groups were formed as a result of the successful deacetylation process, indicating that CA-HBA was successfully converted into the RC-HBA structure without altering its chemical structure.³⁰

Sensing of an OP Pesticide, DFP. In this study, dihydroxy benzaldehyde was conjugated with the DA monomers to synthesize the ester PCDA-HBA (Figure 1), which was then encapsulated in a CA matrix polymer using the electrospinning technique. The as-spun NCF membranes were then hydrolyzed to obtain colorless RC-based PCDA-HBA composites. The resulting solid-state RC-based PCDA-HBAs were then polymerized to PDA-HBAs with 254 nm UV light irradiation. The UV irradiation resulted in an obvious color change from colorless to blue in the PDA composites, which indicated the formation of the π -conjugated backbone of the PDA structure. The blue color was visible within seconds in ambient conditions. The resulting modified polymer responds to the existence of OP toxins in its surrounding environment. Upon exposure to the OP pesticide DFP, the nanocomposites immediately transformed from blue to pink/red, which was clearly visible to the naked eyes (Figure 4).

Effect of PDA-HBA Loading on DFP Sensing. The effect of PDA-HBA loading in the NCFs and the concentration of DFP needed for color transition was investigated thoroughly. The color transition from blue to pink/red was observed as soon as the DFP solution touched the fiber surface, regardless of the amount of PDA-HBA loaded in the NCFs. Although all the composites effectively detected DFP, the PDA-HBA-10 composite, which contains 10% PDA-HBA in its structure, exhibited the most successful results among the four fiber categories studied in this study (Table 1). The most prominent color transition was also observed in PDA-HBA-10 composites, confirming that this composition is optimal for developing RC-based PDA sensors for detecting DFP. Furthermore, the finer fibers developed with HBA-10 may have contributed to the increased sensitivity

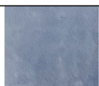
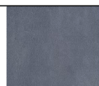
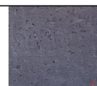
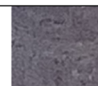



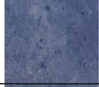
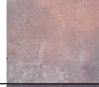
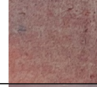


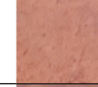

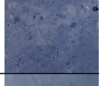

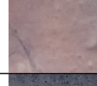

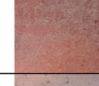
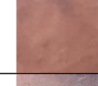








Nanocomposites fibers	DFP concentration						
	Blank	0.01 M	0.05 M	0.1 M	0.20 M	0.4 M	0.6 M
HBA-5							
HBA-10							
HBA-15							
HBA-20							

Figure 4. CL responses of the NCF sensors at various concentrations of OP pesticide DFP.

due to their higher surface area compared with the other composites (Figure 4).³¹

Test of Sensitivity. The effect of the DFP concentration on sensing was also studied in detail with all four types of nanocomposites, including HBA-5, HBA-10, HBA-15, and HBA-20. All of the composites were highly sensitive at DFP concentration above 0.2 M. Below this concentration, the composites began to show differentiate in their responses. HBA-5, with a low PDA ester concentration, exhibited a poor response in the low DFP concentration range. However, HBA-10 composites exhibited the best results, showing an immediate color change to pink/red at DFP concentrations of 0.01 M (100 ppm) and over. As shown in Figure 4, the significant blue-to-pink/red color transition was visible to the naked eyes. As the dermal lethal dose (LD_{50}) of DFP is 117 ppm for a test rabbit,³² the CL response of our first solid-state NCF sensor demonstrated high sensitivity with a prompt response.

To quantify the sensitivity, the samples were evaluated with a UV–vis spectrophotometer. Figure 5A shows the represen-

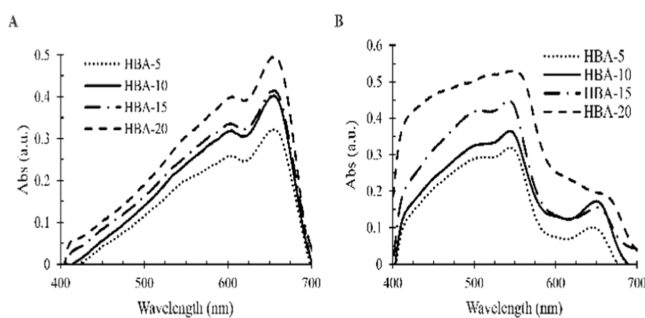


Figure 5. UV–visible spectrophotometer reading of the blue RC–PDA–HBA NCF membranes before color transformation (A) and after color transition (B) upon exposure to 0.6 M DFP in acetone.

tative spectra of the NCFs in the blue state, and spectra in 5B shows the fibers in the pink/red form after color transition upon exposure to DFP. All the composites in the blue state exhibited peaks around 640 nm. However, due to the interaction of the composites with DFP upon exposure, the peak at 640 nm gradually diminished or decreased in intensity. A new peak developed around 560 nm, indicating the red state of the sensing polymer, PDA ester.^{12,20} Therefore, the CL

changes of the PDA ester in solid-state nanocomposites from blue to pink and red are highly promising for OP sensing applications.

An index of the color change, CL response % CR, was calculated from the spectra using eqs 1 and 2, following the established protocol in the literature. The calibration curve is presented in Figure 6. It is evident from the figure that all of

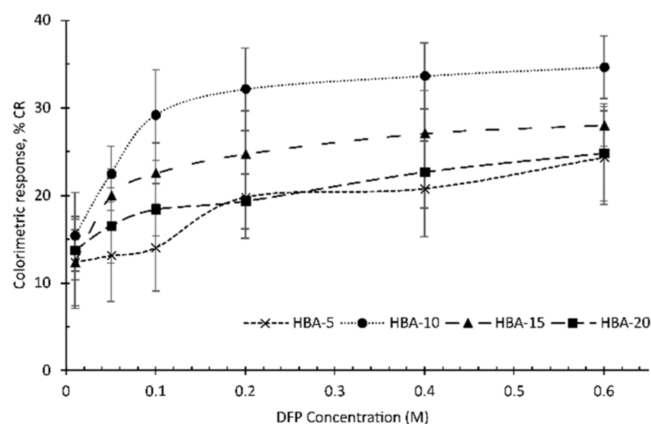


Figure 6. CL response of the composites upon exposure to DFP at various concentrations.

the composites started the color transition at the lowest concentration (1 mmol) experimented with. The CL response increased with the increase of DFP concentration and made a plateau at around 0.2 M. However, the change in CR value below 0.1 M DFP was found to be very little. Similar to visual detection, HBA-10 exhibited the best %CR value. The LOD, the minimum concentration of DFP required to demonstrate a detectable response, was calculated from this calibration curve following the published literature.³³ The CL response was linear from 0.01 to 0.1 M and was used to calculate the LOD. The linear regression curve (Figure S4) of % CR values of HBA-10 can be expressed as $Y = 152.7 \times X + 14.2$, and the calculated LOD was found to be 63 ppm.

Test of Selectivity. The selective detection of the target pesticide is a prime concern for developing pesticide sensors. The selectivity of the developed detection system was examined using some carefully selected potential interferents such as acetone, acetonitrile, water, and HCl to eliminate any

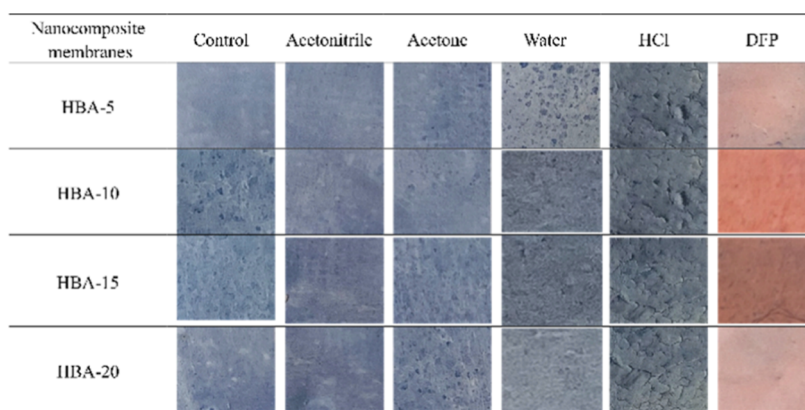


Figure 7. Test of selectivity: response of the nanocomposite membranes to some common confounding chemicals alongside DFP.

possible false alarms of the detection system.^{12,20} This test was planned to examine whether the color change was induced by any solvent used to dissolve or dilute the pesticide or if the color change was induced selectively by DFP only. Acetone, acetonitrile, and water were selected for being commonly used solvents for dissolving or diluting DFP to rule out the possibility of a false positive signal during DFP detection due to the solvents. HCl is a byproduct of the aqueous decomposition of DFP. Therefore, HCl was used to rule out the possibility of color change due to the byproducts of the aqueous decomposition of DFP. Moreover, they mimic the acidic environments found in polluted aqueous sources, where the byproducts of air and water pollution persist.

Figure 7 presents photographs of the PDA–HBA composites before and after exposure to some confounding test chemicals. It is observed from Figure 7 that the blue to red/pink color transition occurred only in the presence of DFP. No visible color change was observed due to the presence of any other chemical species, i.e., acetone, acetonitrile, water, or HCl. Therefore, we inferred that the color transition of PDA–HBA containing NCFs is highly selective to the DFP only; neither the solvents nor the byproducts can induce a color transition. The quantitative response produced by these confounding chemicals, calculated as % blue, is presented in Figure S5.

Mechanism of Color Change during OP Detection. PDAs make up a class of π -conjugated polymers with optical transitioning properties. The DA monomers undergo a 1,4 addition photopolymerization upon irradiation with ultraviolet light, X-rays, or γ -radiation. The irradiation gives a PDA with an alternating ene-yne backbone, and the monomer-to-polymer conversion is accompanied by a visible color change from colorless to blue. The most widely reported mechanism of the topochemical polymerization of the DAs is known as the “turnstile” mechanism. According to this mechanism, when the monomers are exposed to radiation, they pivot approximately 1 Å around the centroid of the DA at 30° to bring carbon atoms C1 and C4 together to create a new bond.³⁴ The monomer-to-polymer transition of DAs is accompanied by a color change from colorless to blue due to the formation of a conjugated ene-yne chromophore.

Herein, we explored the color transition mechanism from blue to red upon exposure to an external stimulus. We employed characterization techniques to gain a better mechanistic understanding of the morphological, structural, and spectral changes of the PDA–HBA composites upon

exposure to DFP. The surface compositions and morphological integrity of the PDA–HBA containing NCF membranes before and after the color change were investigated with SEM coupled with EDS using HBA-10 as a model. The morphologies presented in Figure S6 show that the composites retained their randomly packed continuous morphology irrespective of the color, meaning no morphological change occurred due to the color change.

The elemental composition obtained from EDS is presented in Table 2 and Figure 8. The elemental composition of the

Table 2. Elemental Analysis of the NCFs Before and After Treatment with DFP^a

NCF membranes	elements, %		
	C	O	P
before DFP treatment	72.81 ± 2.96	26.82 ± 3.11	----
after DFP treatment	62.73 ± 2.88	25.83 ± 3.84	1.25 ± 0.23

^aNote. “----” indicates “not present”.

NCFs was changed after the DFP treatment. The blue composites contained their organic elements, i.e., C and O only. However, the elemental composition of the red composites exhibited the presence of phosphorus (P) elements along with C and O, providing evidence of the OP (DFP) treatment of the composites. The sulfur element might be from the impurities of the reagents, and the sodium could be the residual elements from the hydrolysis treatment.³² It is evident from Table 2 that the carbon content decreased from 72.81% to 62.73% in the red composites. The introduction of a characteristic P element at 1.25% in the red state indicates the presence of a P element on the surface of PDA-containing composites.³⁵ These observations suggest that the color change was influenced by the presence of P from DFP found on the membrane surface.

The ¹H NMR of the PCDA–HBA crystal and HBA-10 composites (before and after DFP exposure) was conducted to study if the DFP was structurally integrated into the composites to bring out color transformation. The spectra are presented in Figures S1–S3. The peak assignment can be done as follows: ¹H NMR (400 MHz, DMSO-*d*₆): δ 0.85 (t, 3H), 1.23–1.63 (m, 32H), 2.26 (t, 4H), 2.51 (t, 2H), 6.68–6.75 (m, 2H), 7.68 (s, 1H), and 10.21 (s, 1H). The peak at 0.85 ppm represents the methyl (–CH₃) group; the multiple peaks between 1.23 and 1.63 ppm represent the methylene group (–CH₂–) of the hydrocarbon chain; the peaks at 2.26 and 2.51

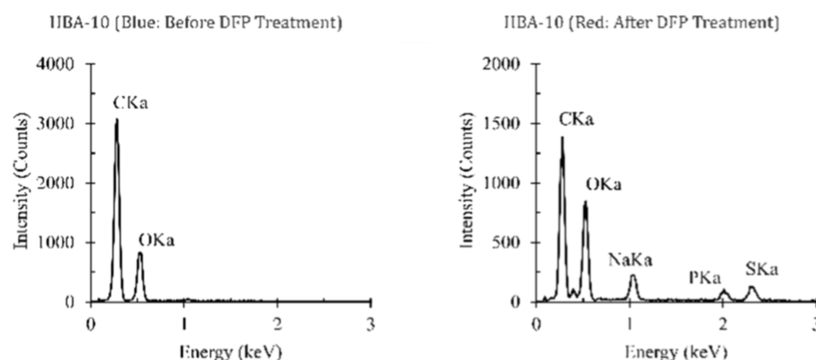


Figure 8. Elemental distribution of the NCF membranes before and after treatment with DFP.

ppm relate to the methylene group adjacent to the alkyne ($-C\equiv$) group; the peaks between 6 and 8 ppm belong to the protons attached to the aromatic ring, and the peak at 10.21 ppm belongs to the aldehyde group added to the PCDA main chain. The spectra are consistent with those in the previously published literature.²⁰

Comparing the spectra of the PCDA–HBA crystal (Figure S1), the blue NCF membranes before the color change (Figure S2), and red NCF membranes after the color change (Figure S3), we determined that the PDA–HBA retains its structural integrity even after the color change, meaning there is no proof of a structural change in the composites.

The XRD measurements were performed to investigate structural or crystallinity changes associated with the chromatic transition in NCF membranes. The X-ray diffractograms of HBA-10 in blue and red phases are presented in Figure 9. The

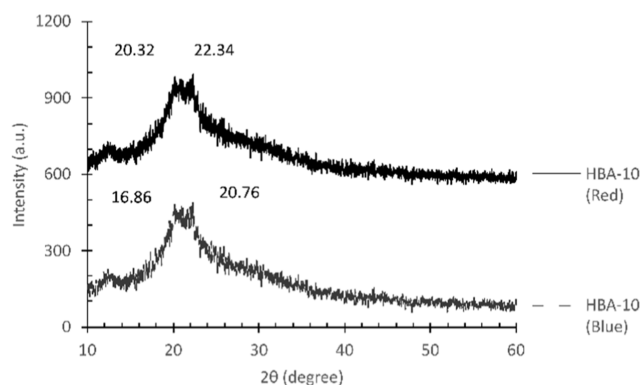


Figure 9. XRD spectra of PDA containing NCF membrane before color change (blue) and after color change (red) due to the exposure to DFP.

results indicate that the PDA containing RC NCF membranes in the blue phase exhibits an amorphous nature, having very low crystallinity. The broad diffraction peaks between 16.86 and 20.76° are characteristic of PDA macromolecules. These peaks align with previously reported patterns in the literature.^{26,36} The characteristic PDA peaks were shifted to 20.32 and 22.34° in the red phase, indicating a shift toward a more crystalline structure due to the color transformation.^{26,36}

This structural reorganization suggests an increase in the order of the material, possibly due to enhanced packing of PDA chains or changes in the alignment of the polymer backbone and side chains. Such shifts have been previously attributed to the distortion of the conjugated PDA backbone caused by external stimuli, leading to the modification of the side chain

crystallinities.^{26,36,37} This phenomenon provides a structural explanation for the observed chromatic transition from blue to red and demonstrates that the optical response is linked to nanoscale structural rearrangements.

These findings are further corroborated by small angle XRD (SAXS) analysis, as presented in Figure 10. The SAXS results

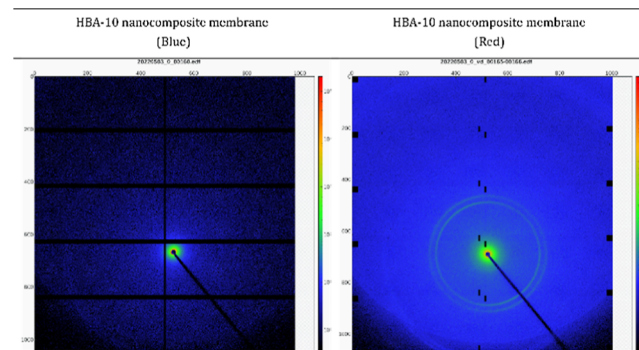


Figure 10. SAXS patterns of HBA-10 NCF membranes before and after color change.

revealed similar trends, where the blue fibers did not show any crystallinity. In contrast, the appearance of the circles around the probe in red fibers indicates a change in crystallinity after the color transformation.

The FT-IR spectra of the blue and red phase HBA-10 nanocomposites were compared and are presented in Figure 11. The diagnostic region of the spectra demonstrates that the composites retain their structural characteristics even after

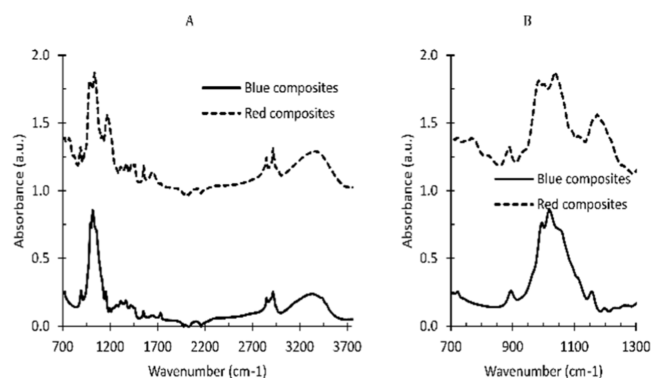


Figure 11. FT-IR spectra of the HBA-10 nanocomposite membranes in blue and red color (A) and the fingerprint regions of the spectra (B).

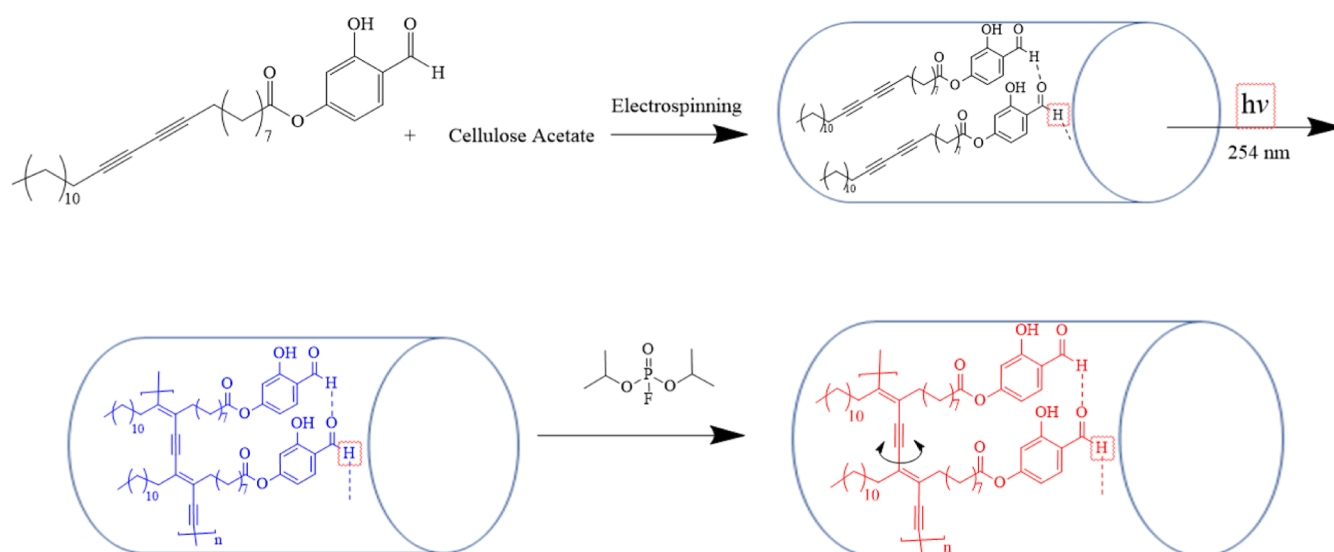


Figure 12. Schematic representation of the NCF sensor development and color transformation of the sensor from blue to red upon exposure to OP pesticide, DFP.

color transformation, suggesting no significant change in the polymer backbone. However, the increase of intensity and a shift to a higher wavenumber of the band at 1683 cm^{-1} of the red phase HBA-10 nanocomposite indicate the development of hydrogen bonding. Moreover, the broadening of the bending band on the fingerprint region at 1036 cm^{-1} and increased intensity of the bending band at 1173 cm^{-1} are also an indication of the development of hydrogen bonding on the PDA macromolecular chain.^{26,38} Therefore, the FT-IR results, along with XRD and SAX observations, suggest a change in PDA conformation associated with color transformation from blue to red/pink. The change in conformation might have resulted in a change in the electronic properties of the PDA macromolecule, resulting in a color transition. The proposed mechanism is depicted in Figure 12.

The mechanism underlying the chromatic transformation of PDAs remains a topic of ongoing discussion among researchers across disciplines.³⁹ When PDA composites are exposed to external stimuli, structural strain is induced within the structure, leading to distortions within the conjugated polymer backbone. This distortion results in a distinct chromic shift from blue (absorption maximum of $\sim 640\text{ nm}$) to red (absorption maximum of $\sim 500\text{ nm}$), corresponding to changes in chain conformations and molecular ordering.⁴⁰ Crystallographic studies suggested that rotations around the C–C bonds within a PDA assembly due to external strain cause chain conformations.⁴¹

The C–C rotations break the planarity of the conjugated backbone, which disrupts the delocalization of the π orbitals. As a result, the highest occupied molecular orbital–lowest unoccupied molecular orbital energy gap is widened to allow the PDA to absorb light at higher energy.^{14,42} The chromatic shift of PDA from blue to red correlates with a planar structure adopting a nonplanar conformation with rotated or distorted side chains.⁴³ Modifying the PCDA carboxylic acid headgroup with other strong groups, such as an amine or aromatic ring, reduces the strain on the conjugated backbone and enhances hydrogen-bonding interactions.^{42,44} Therefore, the observations in FTIR, XRD, and SAX of the PDA–HBA nanocomposite membranes in this study reflected distinctive conformational changes from the blue to red phase during

the chromatic transitions, as suggested by fellow researchers in the field.

CONCLUSIONS

PDA functionalized PCDA ester, PCDA–HBA, was synthesized using a novel green chemistry approach for CL sensing of OP pesticide DFP. Different amounts of PCDA–HBA containing NCFs were successfully fabricated via the electrospinning technique using CA as a matrix polymer. HBA-10 composites, containing 10% (w/w) PCDA–HBA, were the finest fibers spun, having a $0.82 \pm 0.47\text{ }\mu\text{m}$ average fiber diameter. The composites were then chemically hydrolyzed to convert CA composites to RC composites. The generation of a large number of hydroxyl groups on the NF composites made the fibers suitable for DFP sensing. Moreover, the functional groups introduced in the PCDA macromolecule remained unaffected after the hydrolysis process. The RC-based PDA ester containing nanocomposites selectively detected OP pesticide DFP within seconds of exposure to the pesticide, which was visible to the naked eye. The LOD was 63 ppm. The selectivity test involving other confounding chemical species, including acetone, acetonitrile, water, and HCl, revealed that the DFP detection of the nanocomposites was not affected by the presence of any solvent or byproducts. Although no morphological change in the fibers occurred due to the color change, the presence of P atoms was identified on the fibers. No evidence of any new chemical bond formation after the color transformation was identified. However, a decrease in crystallite order and arrangement in the polymer chain, due to the development of hydrogen bonding, was suggested to be the mechanism of the color change. This research study opens a new window toward developing a solid-state nanocomposite-based OP pesticide sensing platform and contributes to protecting human health and saving lives.

ASSOCIATED CONTENT

Supporting Information

The Supporting Information is available free of charge at <https://pubs.acs.org/doi/10.1021/acsomega.4c11365>.

Additional ^1H NMR spectra of sensing polymer PCDA–HBA crystal, composite fibers before DFP exposure, composite fibers after DFP exposure, and DFP in MeOD; calibration curve for calculating LOD; CL response of the composite fiber membranes upon exposure to confounding chemicals; and SEM–EDS images of the composite fibers before and after DFP treatment (PDF)

AUTHOR INFORMATION

Corresponding Author

Chunhui Xiang – Department of Apparel, Events, and Hospitality Management, Iowa State University, Ames, Iowa 50011, United States; orcid.org/0000-0002-8570-1863; Email: chxiang@iastate.edu

Author

A K M Mashud Alam – Department of Apparel, Events, and Hospitality Management, Iowa State University, Ames, Iowa 50011, United States; orcid.org/0000-0003-3629-2669

Complete contact information is available at:

<https://pubs.acs.org/10.1021/acsomega.4c11365>

Author Contributions

The manuscript was written through the contributions of all authors. All authors have given approval to the final version of the manuscript.

Funding

The authors would like to thank the Intramural Collaborative Seed Grants program provided by the author's institute for their financial support.

Notes

The authors declare no competing financial interest.

ACKNOWLEDGMENTS

The authors thank Aleksei V. Ananin and Sharifur Rahman for their help in NMR and Chemdraw.

REFERENCES

- (1) Li, X.; Cui, H.; Zeng, Z. A. Simple Colorimetric and Fluorescent Sensor to Detect Organophosphate Pesticides Based on Adenosine Triphosphate-Modified Gold Nanoparticles. *Sensors* **2018**, *18* (12), 4302.
- (2) García-García, C. R.; Parrón, T.; Requena, M.; Alarcón, R.; Tsatsakis, A. M.; Hernández, A. F. Occupational Pesticide Exposure and Adverse Health Effects at the Clinical, Hematological and Biochemical Level. *Life Sci.* **2016**, *145*, 274–283.
- (3) Namulanda, G.; Monti, M. M.; Mulay, P.; Higgins, S.; Lackovic, M.; Schwartz, A.; Prado, J. B.; Waltz, J.; Mitchell, Y.; Calvert, G. M. Acute Nonoccupational Pesticide-Related Illness and Injury - United States, 2007–2011. *MMWR Morb. Mortal. Wkly. Rep.* **2016**, *63* (55), 5.
- (4) Kim, K.-H. H.; Kabir, E.; Jahan, S. A. Exposure to Pesticides and the Associated Human Health Effects. *Sci. Total Environ.* **2017**, *575*, 525–535.
- (5) Mostafalou, S.; Abdollahi, M. The Link of Organophosphorus Pesticides with Neurodegenerative and Neurodevelopmental Diseases Based on Evidence and Mechanisms. *Toxicology* **2018**, *409*, 44–52.
- (6) Calvert, G. M.; Beckman, J.; Prado, J. B.; Bojes, H.; Schwartz, A.; Mulay, P.; Leinenkugel, K.; Higgins, S.; Lackovic, M.; Waltz, J.; Stover, D.; Moraga-Mchaley, S. *Acute Occupational Pesticide-Related Illness and Injury - United States, 2007–2011*; US Department of Health and Human Services/ Centers for Disease Control and Prevention: GA, USA, 2016; p 11.
- (7) Yan, X.; Li, H.; Su, X. Review of Optical Sensors for Pesticides. *TrAC, Trends Anal. Chem.* **2018**, *103*, 1–20.
- (8) Rawtani, D.; Khatri, N.; Tyagi, S.; Pandey, G. Nanotechnology-Based Recent Approaches for Sensing and Remediation of Pesticides. *J. Environ. Manage.* **2018**, *206*, 749–762.
- (9) Walton, I.; Davis, M.; Munro, L.; Catalano, V. J.; Cragg, P. J.; Huggins, M. T.; Wallace, K. J. A Fluorescent Dipyrinone Oxime for the Detection of Pesticides and Other Organophosphates. *Org. Lett.* **2012**, *14* (11), 2686–2689.
- (10) Aragay, G.; Pino, F.; Merkoçi, A. Nanomaterials for Sensing and Destroying Pesticides. *Chem. Rev.* **2012**, *112* (10), 5317–5338.
- (11) Alam, A. M.; Yapor, J. P.; Reynolds, M. M.; Li, Y. V. Study of Polydiacetylene-Poly (Ethylene Oxide) Electrospun Fibers Used as Biosensors. *Materials* **2016**, *9* (3), 202.
- (12) Zhang, Y.; Bromberg, L.; Lin, Z.; Brown, P.; Van Voorhis, T.; Hattton, T. A. Polydiacetylene Functionalized with Charged Termini for Device-Free Colorimetric Detection of Malathion. *J. Colloid Interface Sci.* **2018**, *528*, 27–35.
- (13) Weston, M.; Tjandra, A. D.; Chandrawati, R. Tuning Chromatic Response, Sensitivity, and Specificity of Polydiacetylene-Based Sensors. *Polym. Chem.* **2020**, *11* (2), 166–183.
- (14) Khanantong, C.; Charoenthai, N.; Wacharasindhu, S.; Sukwattanasitt, M.; Traiphon, N.; Traiphon, R. Influences of Solvent Media on Chain Organization and Thermochromic Behaviors of Polydiacetylene Assemblies Prepared from Monomer with Symmetric Alkyl Tails. *J. Ind. Eng. Chem.* **2018**, *58*, 258–265.
- (15) Pankaew, A.; Traiphon, N.; Traiphon, R. Tuning the Sensitivity of Polydiacetylene-Based Colorimetric Sensors to UV Light and Cationic Surfactant by Co-Assembling with Various Polymers. *Colloids Surf., A* **2021**, *608* (September 2020), 125626.
- (16) Wang, D. E.; Zhang, Y.; Li, T.; Tu, Q.; Wang, J. Self-Immulative Trigger-Initiated Polydiacetylene Probe for β -Glucuronidase Activity. *RSC Adv.* **2014**, *4* (32), 16820–16823.
- (17) Zhang, Z.; Wei, T.; Chen, Y.; Chen, T.; Chi, B.; Wang, F.; Chen, X. A Polydiacetylenes-Based Colorimetric and Fluorescent Probe for L-Arginine and L-Lysine and Its Application for Logic Gate. *Sensor. Actuator. B Chem.* **2018**, *255*, 2211–2217.
- (18) Siribunbandal, P.; Kim, Y.-H.; Osotchan, T.; Zhu, Z.; Jaisutti, R. Quantitative Colorimetric Detection of Dissolved Ammonia Using Polydiacetylene Sensors Enabled by Machine Learning Classifiers. *ACS Omega* **2022**, *7* (22), 18714–18721.
- (19) Lebègue, E.; Farre, C.; Jose, C.; Saulnier, J.; Lagarde, F.; Chevalier, Y.; Chaix, C.; Jaffrezic-Renault, N. Responsive Polydiacetylene Vesicles for Biosensing Microorganisms. *Sensors* **2018**, *18* (2), 599.
- (20) Lee, J.; Seo, S.; Kim, J. Colorimetric Detection of Warfare Gases by Polydiacetylenes toward Equipment-Free Detection. *Adv. Funct. Mater.* **2012**, *22* (8), 1632–1638.
- (21) Zamora-Sequeira, R.; Starbird-Pérez, R.; Rojas-Carillo, O.; Vargas-Villalobos, S. What Are the Main Sensor Methods for Quantifying Pesticides in Agricultural Activities? A Review. *Molecules* **2019**, *24* (14), 2659.
- (22) Jeon, H.; Lee, J.; Kim, M. H.; Yoon, J. Polydiacetylene-Based Electrospun Fibers for Detection of HCl Gas. *Macromol. Rapid Commun.* **2012**, *33* (11), 972–976.
- (23) Wu, X.; Kuruba, R.; Reddy, D. S. Midazolam-Resistant Seizures and Brain Injury after Acute Intoxication of Diisopropylfluorophosphate, an Organophosphate Pesticide and Surrogate for Nerve Agents. *J. Pharmacol. Exp. Ther.* **2018**, *367* (2), 302–321.
- (24) Alam, A.; Jenks, D.; Kraus, G. A.; Xiang, C. Synthesis, Fabrication, and Characterization of Functionalized Polydiacetylene Containing Cellulose Nanofibrous Composites for Colorimetric Sensing of Organophosphate Compounds. *Nanomaterials* **2021**, *11* (8), 1869.
- (25) Rieger, K. A.; Thyagarajan, R.; Hoen, M. E.; Yeung, H. F.; Ford, D. M.; Schiffman, J. D. Transport of Microorganisms into Cellulose Nanofiber Mats. *RSC Adv.* **2016**, *6* (29), 24438–24445.
- (26) Moazeni, N.; Sadrjani, M.; Merati, A. A.; Latifi, M.; Rouhani, S. Effect of Stimuli-Responsive Polydiacetylene on the Crystallization

- and Mechanical Properties of PVDF Nanofibers. *Polym. Bull.* **2020**, *77* (10), 5373–5388.
- (27) de Almeida, D. S.; Duarte, E. H.; Hashimoto, E. M.; Turbiani, F. R. B.; Muniz, E. C.; de Souza, P. R. de S.; Gimenes, M. L.; Martins, L. D. Development and Characterization of Electrospun Cellulose Acetate Nanofibers Modified by Cationic Surfactant. *Polym. Test.* **2020**, *81*, 106206.
- (28) Vatanpour, V.; Pasaoglu, M. E.; Barzegar, H.; Teber, O. O.; Kaya, R.; Bastug, M.; Khataee, A.; Koyuncu, I. Cellulose Acetate in Fabrication of Polymeric Membranes: A Review. *Chemosphere* **2022**, 295 (January), 133914.
- (29) Wu, J.; Quan, Z.; Zhang, H.; Qin, X.; Wang, R.; Yu, J. Electrospun Cellulose Acetate Nanofiber Upscaling with a Metal Plate Needleless Spinneret. *Mater. Res. Express* **2019**, *6* (12), 1250e4.
- (30) Alam, A. K. M. M.; Ewaldz, E.; Xiang, C.; Qu, W.; Bai, X. Tunable Wettability of Biodegradable Multilayer Sandwich-Structured Electrospun Nanofibrous Membranes. *Polymers* **2020**, *12* (9), 2092.
- (31) Kim, J. H.; Lee, J. S. Development of Polydiacetylene Embedded Polyurethane Nanocomposites as a Mask for Sensing and Filtering Fine Dust. *Fibers Polym.* **2021**, *22* (2), 489–497.
- (32) Aldrich, S. Safety Data Sheet Diisopropylfluorophosphate. <https://www.sigmaaldrich.com/US/en/sds/sigma/d0879> (accessed 06-20-2022).
- (33) Pham, T. B.; Hoang, T. H. C.; Pham, V. H.; Nguyen, V. C.; Van Nguyen, T.; Vu, D. C.; Pham, V. H.; Bui, H. Detection of Permethrin Pesticide Using Silver Nano-Dendrites SERS on Optical Fibre Fabricated by Laser-Assisted Photochemical Method. *Sci. Rep.* **2019**, *9* (1), 12590.
- (34) Lauher, J. W.; Fowler, F. W.; Goroff, N. S. Single-Crystal-to-Single-Crystal Topochemical Polymerizations by Design. *Acc. Chem. Res.* **2008**, *41* (9), 1215–1229.
- (35) Qin, M.; Yao, B.; Shi, Q.; Tang, W.; Chen, S.; Guo, T.; Wang, W.; Zhang, Y.; Ge, Z. PDA Modification and Properties of α - AlH 3. *Sci. Rep.* **2022**, *12* (1), 12348.
- (36) Ye, Q.; You, X.; Zou, G.; Yu, X.; Zhang, Q. Morphology, Structure and Chromatic Properties of Azobenzene-Substituted Polydiacetylene Supramolecular Assemblies. *J. Mater. Chem.* **2008**, *18* (24), 2775–2780.
- (37) Nyayachavadi, A.; Langlois, A.; Tahir, M. N.; Billet, B.; Rondeau-Gagné, S. Conjugated Polymer with Polydiacetylene Cross-Links through Topochemical Polymerization of 1,3-Butadiyne Moieties Toward Photopatternable Thin Films. *ACS Appl. Polym. Mater.* **2019**, *1* (7), 1918–1924.
- (38) Ramírez-Hernández, A.; Aguilar-Flores, C.; Aparicio-Saguilán, A. Fingerprint Analysis of FTIR Spectra of Polymers Containing Vinyl Acetate. *Dyna* **2019**, *86* (209), 198–205.
- (39) Hall, A. V.; Musa, O. M.; Steed, J. W. Properties and Applications of Stimuli-Responsive Diacetylenes. *Cryst. Growth Des.* **2021**, *21* (6), 3614–3638.
- (40) Jelinek, R.; Ritenberg, M. Polydiacetylenes-Recent Molecular Advances and Applications. *RSC Adv.* **2013**, *3* (44), 21192–21201.
- (41) Carpick, R. W.; Sasaki, D. Y.; Marcus, M. S.; Eriksson, M. A.; Burns, A. R. Polydiacetylene Films: A Review of Recent Investigations into Chromogenic Transitions and Nanomechanical Properties. *J. Phys.: Condens. Matter* **2004**, *16* (23), R679–R697.
- (42) Khanantong, C.; Charoenthai, N.; Kielar, F.; Traiphol, N.; Traiphol, R. Influences of Bulky Aromatic Head Group on Morphology, Structure and Color-Transition Behaviors of Polydiacetylene Assemblies upon Exposure to Thermal and Chemical Stimuli. *Colloids Surf., A* **2019**, *561* (November 2018), 226–235.
- (43) Scoville, S. P.; Shirley, W. M. Investigations of chromatic transformations of polydiacetylene with aromatic compounds. *J. Appl. Polym. Sci.* **2011**, *120* (5), 2809–2820.
- (44) Tanioku, C.; Matsukawa, K.; Matsumoto, A. Thermochromism and Structural Change in Polydiacetylenes Including Carboxy and 4-Carboxyphenyl Groups as the Intermolecular Hydrogen Bond Linkages in the Side Chain. *ACS Appl. Mater. Interfaces* **2013**, *5* (3), 940–948.